Development 133, 4463-4473 (2006) doi:10.1242/dev.02647

Essential pro-Bmp roles of crossveinless 2 in mouse organogenesis

Makoto Ikeya[1], Masako Kawada[1], Hiroshi Kiyonari[2], Noriaki Sasai[1], Kazuki Nakao[2], Yasuhide Furuta[3] and Yoshiki Sasai[1,*]

We here report essential roles of the Bmp-binding protein crossveinless 2 (Cv2; Bmper) in mouse organogenesis. In the null *Cv2* mutant mouse, gastrulation occurs normally, but a number of defects are found in *Cv2*-expressing tissues such as the skeleton. Cartilage differentiation by Bmp4 treatment is reduced in cultured $Cv2^{-/-}$ fibroblasts. Moreover, the defects in the vertebral column and eyes of the $Cv2^{-/-}$ mouse are substantially enhanced by deleting one copy of the *Bmp4* gene, suggesting a pro-Bmp role of *Cv2* in the development of these organs. In addition, the $Cv2^{-/-}$ mutant exhibits substantial defects in Bmp-dependent processes of internal organ formation, such as nephron generation in the kidney. This kidney hypoplasia is synergistically enhanced by the additional deletion of *Kcp* (*Crim2*) which encodes a pro-Bmp protein structurally related to Cv2. This study demonstrates essential pro-Bmp functions of *Cv2* for locally restricted signal enhancement in multiple aspects of mammalian organogenesis.

KEY WORDS: Crossveinless 2 (Bmper), Mouse, Organogenesis, Gene targeting, Crim2

INTRODUCTION

Embryogenesis is a complex process involving a number of cell-cell interactions mediated by extracellular signals. The Bmp family is a class of extracellular signaling proteins that are well conserved across species, including vertebrates and invertebrates (Hogan, 1996). Bmp proteins were first isolated on the basis of their bone-inducing activity in mammalian tissues (therefore, named bone morphogenetic proteins) and play key regulatory roles in skeletal development (reviewed by Wan and Cao, 2005). Interestingly, the Bmp family signals have been shown to play a variety of roles in the control of embryogenesis, including in cell-type specification, maturation, cell growth, apoptosis and dorsoventral axis determination (Hogan, 1996; De Robertis and Sasai, 1996; Massague and Chen, 2000; Hammerschmidt and Mullins, 2002).

A characteristic feature of Bmp signals is their function as a morphogen; they generate an activity gradient and evoke multiple-threshold responses in recipient cells (Gurdon and Bourillot, 2001). In *Xenopus*, for example, Bmp4 induces the graded ventralization of mesodermal and ectodermal tissues in a dose-dependent manner (Dale et al., 1992; Jones et al., 1992; Fainsod et al., 1994). In *Drosophila*, a gradient of the Dpp (fly Bmp4) activity in the ectoderm determines the dorsoventral specification (Ferguson and Anderson, 1992a; Wharton et al., 1993). Therefore, the fine spatial control of Bmp signals is important for tissue formation to occur in the right place.

Over the past decade, several classes of factors that negatively regulate Bmp signals in the extracellular space have been identified. A typical example is a class of secreted antagonist proteins that bind to and inactivate Bmp proteins, such as noggin, chordin (Chd), follistatin, cerberus and gremlin (Smith and Harland, 1992; Lamb et al., 1993; Sasai et al., 1994; Sasai et al., 1995; Hemmati-Brivanlou et al., 1994; Glinka et al., 1997; Hsu et al., 1998).

Extracellular factors regulate Bmp signals not only negatively but also positively. For example, detailed genetic analyses in the fly have shown that Sog (fly Chd) functions both as an antagonist (anti-Bmp, hereafter) and as a potentiator (pro-Bmp) of Bmp (Dpp) signals in a context-dependent manner. The $sog^{-/-}$ mutant has a strong ventral defect (e.g. reduction of the ventral neurogenic ectoderm) with expanded dorsal non-neural ectoderm (Zusman et al., 1988; Ferguson and Anderson, 1992b; François et al., 1994). In this dorsalization phenotype, Sog is shown to act antagonistically against Dpp (Ferguson and Anderson, 1992b). Nevertheless, the *sog* mutant shows impaired formation of the dorsalmost tissue (amnioserosa), which requires the highest level of Bmp activity (Zusman et al., 1988; Ashe and Levine, 1999; Decotto and Ferguson, 2001). In this particular context, Sog is thought to act as a pro-Bmp factor.

Chd also seems to play some pro-Bmp roles in vertebrate development, although the mechanistic details are poorly understood. In zebrafish, for example, formation of the ventral tail fin, which is a derivative of the ventral-most tissue, requires the highest level of Bmp signaling (Wagner and Mullins, 2002; Rentzsch et al., 2006). The fish *Chd* mutant (*chordino*) has a reduced ventral tail fin (Fisher et al., 1997; Schulte-Merker et al., 1997; Hammerschmidt and Mullins, 2002; Rentzsch et al., 2006), suggesting that Chd is necessary to enhance the Bmp signaling in the ventralmost tissue just as is indicated for fly Sog in the amnioserosa.

Structurally, the Chd/Sog protein contains four cysteine-rich domains. At least two of these domains interact physically with Bmp proteins and play an essential role in inhibiting Bmp activity (Larrain et al., 2000). We have previously reported the isolation of a secreted protein, named kielin, which contains 27 repeats of the Chd-type cysteine-rich domains (Matsui et al., 2000). Kielin is expressed specifically in the dorsal axis (the notochord and floor plate) of the *Xenopus* embryo. Microinjection of *kielin* mRNA weakly promotes paraxial mesoderm differentiation but does not induce strong dorsalization (such as ectopic neural differentiation, which is typical for the Chd-mediated Bmp inhibition in *Xenopus*) (Sasai et al.,

[1]Organogenesis and Neurogenesis Group, Center for Developmental Biology, RIKEN, Kobe 650-0047, Japan. [2]Laboratory for Animal Resources and Genetic Engineering, Center for Developmental Biology, RIKEN, Kobe 650-0047, Japan. [3]Department of Biochemistry and Molecular Biology, M. D. Anderson Cancer Center, University of Texas, Houston, TX 77030, USA.

*Author for correspondence (e-mail: sasaicdb@mub.biglobe.ne.jp)

Accepted 8 September 2006

1995). This raises the possibility that kielin does not simply block Bmp signals, even though it contains numerous cysteine-rich domains.

A mouse database search has identified several kielin/Chd-related factors (see Fig. S1 in the supplementary material). In mammals, Cv2 (Bmper – Mouse Genome Informatics) and kielin-chordin-related protein (Kcp) are the most closely related to kielin among these kielin/Chd-related proteins, and form a subfamily with it (O'Connor et al., 2006). Like kielin, Cv2 and Kcp contain multiple Chd-type cysteine-rich (CR) domains (five and 18 repeats, respectively; see Fig. S1A in the supplementary material). In addition, a von Willebrand factor type D-like (vWD) domain and a trypsin inhibitor-like cysteine-rich (TIL) domain are located at the C terminus of each protein.

cv2 was first identified in the fly mutant study as a gene required for the formation of cross-veins in the fly wing (Garcia-Bellido and de Celis, 1992). Genetic studies in flies showed that the formation of these veins requires high Bmp signaling activity (involving Dpp and Gbb), and that Cv2 is essential for enhancing the local Bmp signal near the receiving cells (O'Connor et al., 2006). This pro-Bmp role of Cv2 was also demonstrated by the reduction of phosphorylated Mad protein in the fly *cv2* mutant (Conley et al., 2000; Ralston and Blair, 2005). In addition, forced expression of *cv2* can antagonize the effect of *sog* overexpression in the wing cross-vein formation (Ralston and Blair, 2005).

By contrast, the in vivo role of the vertebrate counterpart of Cv2 remains rather nebulous. Two opposing activities have been proposed for Cv2. One is to attenuate Bmp signals. Microinjection of *Cv2* mRNA into the *Xenopus* embryo results in the formation of a secondary axis similar to the Chd-induced one (Moser et al., 2003; Coles et al., 2004). In vitro, purified recombinant human CV2 (at excessive doses) inhibits the Bmp-dependent osteoblast and chondrocyte differentiation in cultured cells (Binnerts et al., 2004). Moreover, the transfection of 293T cells with a *Cv2* plasmid reduces cellular response to Bmp4 protein in a Bmp-responding luciferease reporter assay (Moser et al., 2003). The other theory is that Cv2 enhances Bmp signaling, as does its fly homologue. A report (Kamimura et al., 2004) has shown that transfection of a *Cv2* plasmid enhances the cellular response to Bmp4, as measured by Smad phosphorylation. We have also observed that the addition of Cv2 protein (6 nM) enhances Bmp4 (25 nM)-induced cartilage differentiation in cultured E14.5 mouse embryonic fibroblasts (M.I. and Y.S., unpublished). In *Xenopus*, co-injection of *Cv2* and *Bmp4* mRNA into animal pole blastomeres synergistically induces the ectopic expression of *Xbra* (Coles et al., 2004). Thus, these gain-of-function analyses have so far failed to provide a consistent answer to the question 'do vertebrate Cv2 acts as an anti-Bmp or a pro-Bmp factor in embryogenesis?'. Although a recent zebrafish *Cv2* morphant study (Rentzsch et al., 2006) reported a pro-Bmp role in the dorsoventral axis patterning, the same study also indicated that Cv2 protein may acts as an anti-Bmp factor depending on its proteolytic processing, suggesting a possible bidirectional role for vertebrate Cv2.

In the present study, to elucidate the exact role of Cv2 in vivo, we performed a loss-of-function study by generating the 'null' *Cv2* mutant. Based on loss-of-function evidence and genetic interaction data, we demonstrate that Cv2 plays essential roles as a local enhancer of Bmp signals in mouse organogenesis.

MATERIALS AND METHODS

Generation of *Cv2* and *KCP* mutant mice and genetic crossing

The *Cv2* (*tau-lacZ*), *Cv2* (*nlacZ*) and *Kcp* mutants (RIKEN Accession Numbers CDB0402K, CDB0451K and CDB0401K, respectively) were established as follows. *Cv2* and *Kcp* genomic clones were isolated from C57BL/6 genomic phage libraries or BAC libraries. We constructed a targeting vector by inserting *lacZ-neo* cassettes into the *Cv2* or *Kcp* locus, so that the first exon of each gene be replaced with *lacZ* at the first ATG. To generate the *Cv2* (*nlacZ*) knockout line, we constructed a targeting vector using a combined in vivo/in vitro recombination technique (the EG construction method) described previously (Ikeya et al., 2005).

To generate the targeted ES cells, TT2 ES cells (Yagi et al., 1993a) were transfected with the resultant targeting vector made with pMCDT-A(A+T/pau) (Yagi et al., 1993b) and selected with G418. Recombinant ES cells were injected into an eight-cell embryo (inside of the zona pelucida) of CD-1 mice. For the *Cv2* mutant, we obtained a germline chimera from one recombinant line each for *tau-lacZ* and for *nlacZ*. No differences in the null mutant phenotypes were observed between the two mouse lines. The *nLacZ* line gave better β-galactosidase staining (probably because *lacZ* was used instead of *tau-lacZ*), and was used for in vivo expression analysis. For the *Kcp* mutant, we obtained germline chimeras from two independent recombinants. To remove the *pgk-neo* cassette from the *Kcp* mutant genome, pCAG-cre plasmid was injected into the fertilized egg. The correct excision was confirmed by Southern blot analysis.

To detect the *tau-lacZ* knock-in allele of *Cv2*, PCR primers were designed for the sequence upstream and downstream of the start codon of *Cv2* (Cv2-5′ and Cv2-3′, respectively), and for the sequence of *tau* (Cv2-T). The lengths of the amplified cDNA fragments are 564 bp for the wild type and 412 bp for the mutant. The primers are as follows: Cv2-5′, 5′-AGTCGCCCGGGATTC-CCTCCAGGT-3′; Cv2-3′, 5′-AGATGCTGCCTAGCACCGTGGATTT-3′; Cv2-T, 5′- TGTCATCGGGTCCAGTCCCATCTTT-3′. To detect the *nLacZ* knock-in allele of *Cv2*, a primer for β-galactosidase (mCv2-L, 5′-TAACCGTGCATCTGCCAGTTTGAGG-3′) was used. The length of the mutant fragment is 375 bp. To detect the *Kcp* mutant allele, primers were designed for the sequence upstream and downstream of the start codon of *Kcp* (Kcp-5′ and Kcp-3′, respectively), and for the sequence of *tau* sequence (Kcp-T). The lengths of the amplified cDNA fragments are 553 bp for the wild type and 390 bp for the mutant. The primers are as follows: Kcp-5′, 5′-GAGCTTGGAAGACTGCTATGGGTCA-3′; Kcp-3′, 5′-AGCCTCTGCT-TCACCGCTACTTAGG-3′; Kcp-T, 5′-GGTTTCAGAGCCTGGTTCCTC-AGAT-3′. All the lines were backcrossed with C57BL/6 genetic background for two or three generations prior to analysis.

Bmp4 mutant mice (Lawson et al., 1999) were crossed to the *Cv2* mutant strain. To detect the *Bmp4* mutant allele, primers were designed for the sequence upstream and downstream of the start codon of *Bmp4* (Bmp4-5′ and Bmp4-3′, respectively), and for the sequence of sequence of β-galactosidase sequence (Bmp4-L). The lengths of the amplified cDNA fragments are 495 bp for the wild type and about 300 bp for the mutant. The primers are as follows: Bmp4-5′, 5′-GCAGCTGGTGTGTGTGTGTAGGG-3′; Bmp4-3′, 5′-GTTCCCTGGCTCTGCTCTTCCTCCT-3′; Bmp4-L, 5′-TTCACCCAC-CGGTACCTTACGCTTC-3′.

Histology, and skeletal specimen preparation

For histological analyses, embryos were fixed in 7.6% formamide/distilled water or Bouin's fixative overnight. They were then embedded in paraffin, sectioned at 10 μm and stained with Hematoxylin-Eosin (HE) as described previously (Ikeya et al., 1998).

Skeletons were prepared as described previously (Parr and McMahon, 1995). Briefly, E14.5, E18.5 and P0 mice were eviscerated, skinned, fixed in 80% alcohol and stained with Alcian Blue and Alizarin Red.

Immunohistochemistry, immunostaining, whole-mount in situ hybridization and statistics

For immunohistochemistry, samples were fixed in 4% paraformaldehyde/phosphate-buffered saline for 30 minutes and processed as described previously (Mizuseki et al., 2003). Primary antibody dilutions were as follows: anti-human Ki67 at 1:200 (BD Pharmingen, mouse monoclonal), anti-Zic1 at 1:3000 (Su et al., 2006), anti-rat aquaporin 5 (AQP5) at 1:5 (CHEMICON, rabbit polyclonal), anti-Cc10 (T18) at 1:10 (Santa Cruz, goat polyclonal), anti-Hnf3b at 1:100 (DSHB), anti-Isl1 at 1:200 (DSHB), anti-Mash1 at 1:10 (Pharmingen, mouse monoclonal), anti-Msx1/2 at 1:100 (DSHB, 4G1), anti-Pax2 at 1:200 (Babco, rabbit polyclonal), anti-Pax7 at 1:200 (DSHB), anti-Pecam

(CD31) at 1:25 (BD Pharmingen, rat monoclonal), anti-human prosurfactant protein C (proSP-C) at 1:200 (Chemicon, rabbit polyclonal), and anti- smooth muscle actin (SMA) at 1:4000 (Sigma, mouse monoclonal, clone 1A4).

Whole-mount immunostaining was performed with an anti-Wt1 antibody (at 1/100 dilution; Santa-Cruz) and anti-E-cadherin antibody (at 1/500 dilution; TAKARA, ECCD2) as described previously (Grieshammer et al., 2005). In situ hybridization was performed as described previously (Mizuseki et al., 2003).

For the statistical analysis of proliferating chondrocytes, we counted Ki67-positive cells among DAPI-positive cells in a 150 μm × 150 μm square area around the notochord in four to six randomly selected sections of each embryo (three samples for each genotype). The glomeruli in developing kidneys were counted in HE-stained sections that represented the maximum area along the longest axis, and the numbers from six to 16 sections for each genotype were scored.

RT-PCR analysis

RT-PCR was performed as described previously (Mizuseki et al., 2003). The primers used for RT-PCR were as follows:
aggrecan 1, 5′-CCAAGTTCCAGGGTCACTGT-3′ and 5′-CCAAGTTCCAGGGTCACTGT-3′;
Col2a1, 5′-GCCAAGACCTGAAACTCTGC-3′ and 5′-CTTGCCCCACTTACCAGTGT-3′;
Gapdh, 5′-GACCCCTCATTGACCTCAACTACA-3′ and 5′-GGTCTTACTCCTTGGAGGCCATGT-3′;
Cv2, 5′-ATTACCTGCTGCGTCTTGCT-3′ and 5′-TTCTCTCACGCACTGTGTCC-3′;
Pax1, 5′-CACATTCAGTCAGCAACATCCTG-3′ and 5′-TGTATACTCCCTGCTGGTTGGAA-3′.

MEF preparation and induction assays

MEF cells from each embryo were prepared as described previously (Hogan et al., 1994; Lengner et al., 2004) with some modification. Briefly, E14.5 embryos were dissected from heterozygous mouse intercrosses. The trunk tissues of each eviscerated embryo were separately sheared through an 18-G syringe once in 1 ml of 0.05% trypsin/1 mM EDTA/0.001% DNase I and incubated at 37°C for 10 minutes. The cells were plated on one 10 cm tissue culture dish per embryo and culture in DMEM/10% FCS. MEF cells from $Cv2^{+/-}$ mice and those from $Cv2^{-/-}$ mice contained similar percentages of *lacZ*-positive cells (~25%). MEF cells (1×10^5, passage two or three) were plated onto each well of a 24-well cell culture plate (BD Falcon). The recombinant human BMP4 (R&D) was added to the culture 24 hours after plating. RT-PCR was performed 72 hours after plating.

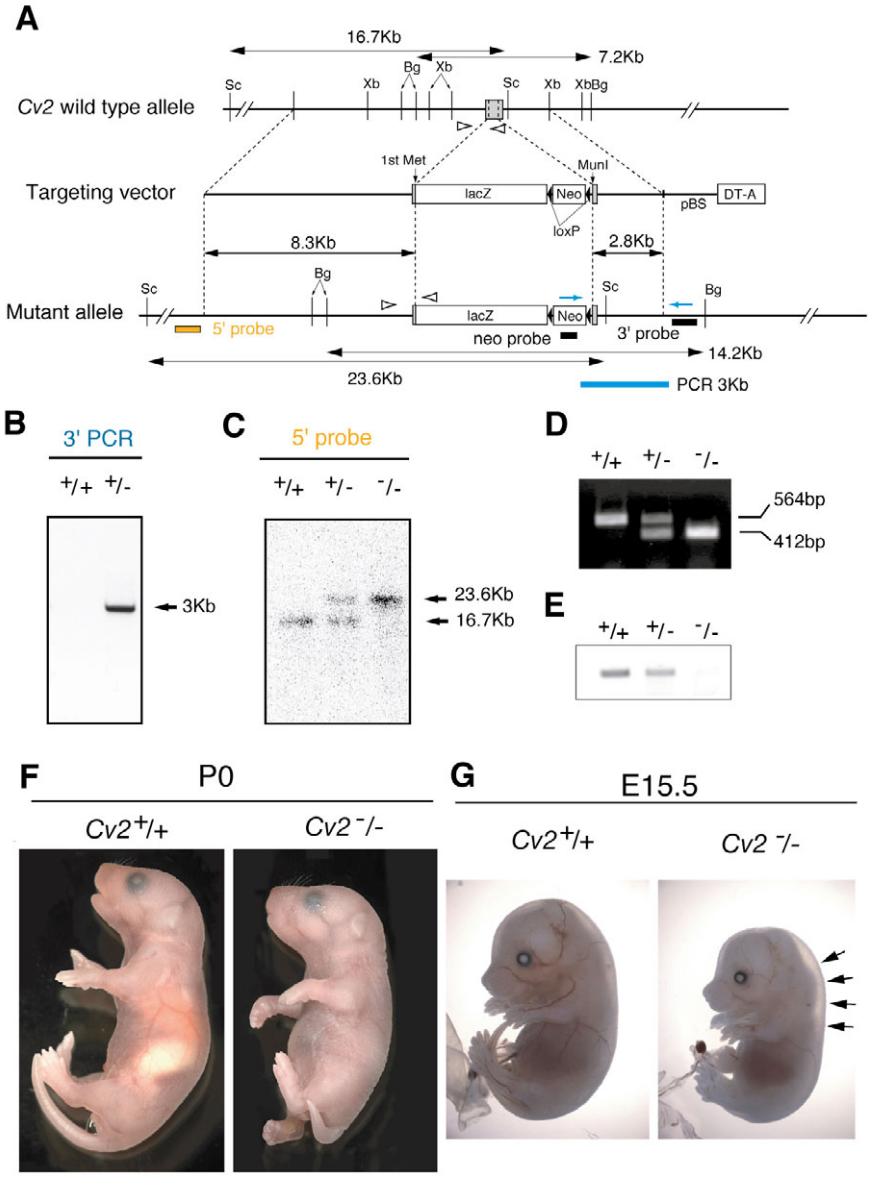

Fig. 1. Generation and external phenotypes of *Cv2* knockout mice. (**A**) Construction of the targeting vector. In the mutant allele, the first methionine of Cv2 was replaced in-frame with that of tau-*lacZ*. The locations of PCR primers used for selection of recombinant ES cells (blue arrows) and genotyping (white arrowheads), and probes for Southern blot analysis (black and orange boxes) are indicated. Bg, *Bgl*II; Sc, *Sac*I; Xb, *Xba*I. (**B**,**C**) Genomic PCR and Southern blot analyses for the homologous recombinant ES cell line. (B) Recombination at the 3′ region of the Cv2 genome (resulting in a 3 kb PCR fragment) was observed. (C) Correct integration was further examined by Southern blot using the 5′ probe (wild-type, heterozygous and homozygous, from left to right lanes). (**D**) PCR genotyping of mutant mice. The wild-type allele band (564 bp) and the mutant allele band (412 bp) were amplified by PCR. (**E**) RT-PCR analysis of *Cv2* expression in E12.5 mutant mice. (**F**,**G**) External appearances of P0 neonates (F) and E15.5 embryos (G). The control mice are on the left side and the null mutant mice are on the right side. At a low penetrance, exencephaly was also observed (arrows) at E15.5 (about 7% of embryos; *n*=86).

RESULTS

Perinatal fatal phenotype in *Cv2*$^{-/-}$ mice

Homologous recombination using a *Cv2*-targeting vector was performed with mouse TT2 embryonic stem (ES) cells (Yagi et al., 1993a) (Fig. 1A,B). Germ-line transmission was obtained with one line of the revertant cells (line 32; Fig. 1C-E), which was used for further analysis. To rule out artifacts resulting from using a single line, we also generated another *Cv2* mutant ES cell line using a different knockout vector with an *nLacZ* insert (see Fig. S2A in the supplementary material). The mutant mice of this second line showed perinatal and embryonic phenotypes (discussed below) that were indistinguishable from those of the first mutant line.

Heterozygous mice exhibited no particular phenotypes. By contrast, homozygous *Cv2*$^{-/-}$ mutants died soon after birth (after breathing several times), and no neonates survived. At and before birth, *Cv2*$^{-/-}$ mutants were found in a reasonable Mendelian ratio (see Table S1 in the supplementary material). At postnatal day 0 (P0), the *Cv2*$^{-/-}$ mutants showed a phenotype of a short trunk and a short curved tail (Fig. 1F). There was no sign of milk intake in the stomach. At embryonic day 15.5 (E15.5), the null mutant mice did not show drastic defects in their external appearance but were generally smaller than the control siblings (Fig. 1G). In addition, a large subcutaneous lucent space was found in the dorsal midline (arrows in Fig. 1G).

Temporal and spatial expression of *Cv2* during embryogenesis

Previous studies have reported *Cv2* expression in embryonic and adult mouse tissues as well as in ES cells (Coffinier et al., 2002; Moser et al., 2003). By using *nLacZ*-knocked-in *Cv2*$^{+/-}$ mice, we analyzed in detail the *Cv2* expression patterns during the organogenetic stages.

At E10.5 (Fig. 2A,B), *Cv2* was expressed in the dorsal midline of the CNS (arrowhead), migrating neural crest (nc), head mesenchyme, trigeminal ganglion (t), otic vesicle (o), para-aortic region and mesonephros (mn). At E11.5 (Fig. 2C,D), strong *Cv2* expression was first detected in the presumptive vertebral body (arrowhead) and arch (arrow). At E14.5 and E18.5 (Fig. 2E-H; data not shown), *Cv2* expression was detected in a number of developing skeletal structures and internal organs, including the vertebral body (vb) and arch (va), ribs (r), skull and long bones, limb girdle bones, pharyngeal and tracheal cartilages, dorsal root ganglion (drg), lung (l; particularly in the developing alveoli), kidney (condensed nephrogenic mesenchyme, or metanephric mesenchyme), and relatively small areas of the CNS. Expression of *Cv2* in the developing nephrons of the kidney was also seen at P0 (Fig. 2I-K; discussed later).

Skeletal defects in *Cv2*$^{-/-}$ mice

The short-trunk phenotype (Fig. 1F,G) promoted us to analyze the skeletal formation in *Cv2*$^{-/-}$ embryos, and multiple defects were observed in bone and cartilage development at P0 (Fig. 3A′; also see Table S2 in the supplementary material). They included in the formation of the vertebrae (Fig. 3B′-F′; discussed below), ribs (lack of the 13th ribs, Fig. 3G′), pharyngeal/tracheal cartilages (small hyoid, thyroid and cricoid cartilages and a lack of tracheal cartilages, Fig. 3A′,J′), skull (a wider unossified area of the metopic suture and small interparietal and supraoccipital bones, Fig. 3K′ and see Table S2 in the supplementary material; a cavity in the basisphenoid bone, Fig. 3L′; loss of the retrotympanic process of the squamosal bone, Fig. 3M′), scapula (small or with a hole in the middle, Fig. 3N′) and humerus (lack of the deltoid tuberosity, Fig. 3N′) and the pubic bone (smaller body of the pubis and unclosed symphysis, Fig. 3O′). In particular, gross defects were found in the vertebral column. When compared with those of the control mice (*Cv2*$^{+/+}$and *Cv2*$^{+/-}$), the vertebral bodies of *Cv2*$^{-/-}$ mice were smaller and showed reduced bone formation throughout the rostrocaudal axis (Fig. 3A′,G′). In addition, the vertebral arches (from the cervical to the sacral regions) were largely missing (Fig. 3B′-F′). Similar vertebral phenotypes were also seen in earlier embryos (E14.5; Fig. 3H′-I′). These vertebral arch defects were not accompanied by the neural tube defect such as an unclosed spinal cord (Fig. 1F,G; see Fig. S4 in the supplementary material).

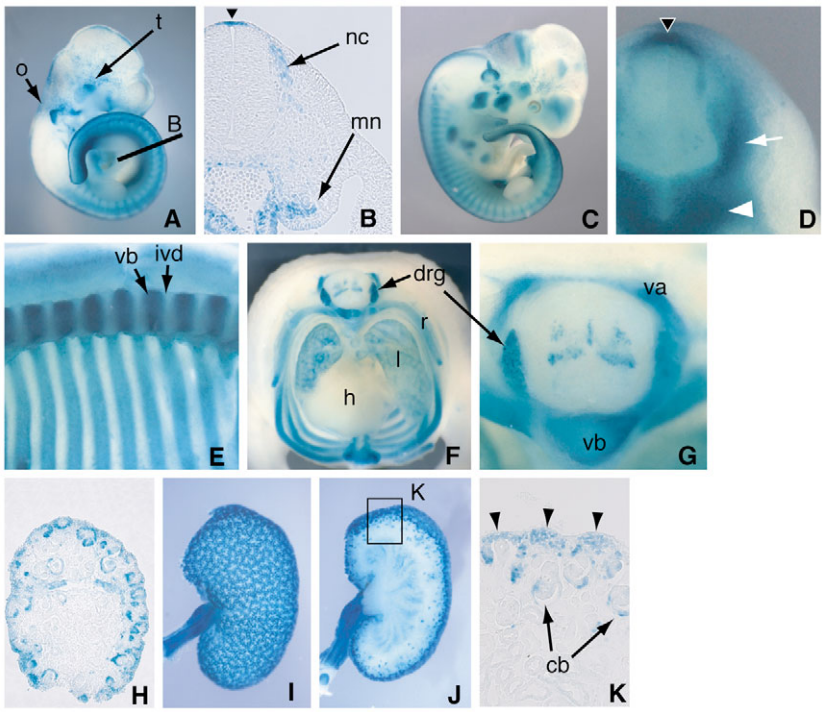

Fig. 2. Expression of *Cv2* analyzed with *nlacZ*-knocked-in mice. (**A**,**B**) At E10.5, *lacZ* staining was observed in the dorsal midline of the neural tube (arrowhead), migrating neural crest (nc), head mesenchyme, trigeminal ganglion (t), otic vesicle (o), para-aortic region and mesonephros (mn). (B) Transverse section at position shown in A. (**C**,**D**) E11.5 embryo. Strong staining appeared in the presumptive vertebral body (arrow) and arch regions (arrowhead). Black arrowhead indicates the dorsal midline of the neural tube. (**E-G**) At E14.5, the staining was observed in the vertebral body (vb), vertebral arch (va), dorsal root ganglion (drg), part of the neural tube, lung (l), heart (h) and ribs (r). (E) Sagittal section of the trunk region, showing that intervertebral discs (ivd) are *lacZ* negative. (G) Higher magnification of the neural tube and vertebra. (**H-K**) Developing kidneys. The condensed nephrogenic mesenchymes were stained with X-gal at E14.5 (H). At P0 (I-K), the staining was observed in the condensed nephrogenic mesenchymes (arrowheads) surrounding the distal tip of the collecting duct, and in the comma-shaped bodies (cb).

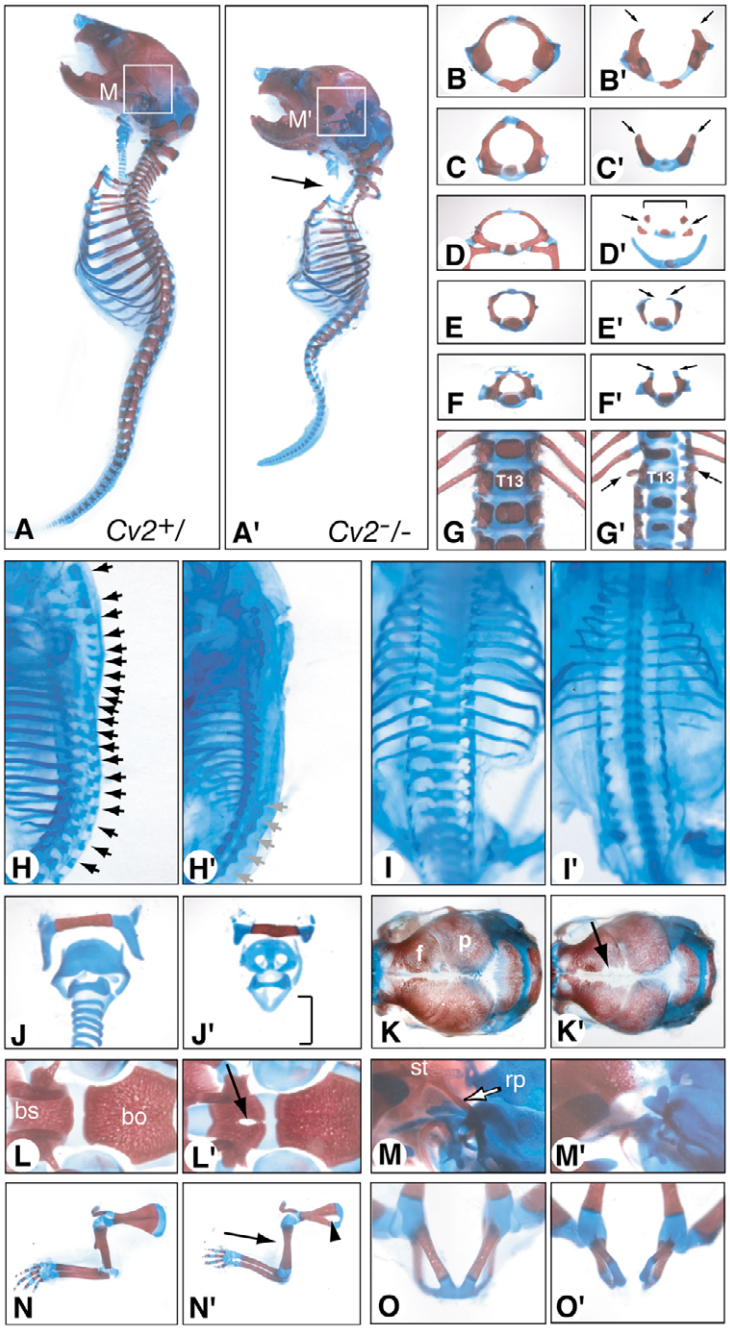

Fig. 3. Skeletal defects in the *Cv2*$^{-/-}$ mice. (A-O) Control littermate and (A′-O′) *Cv2*$^{-/-}$ mutant. (**A**,**A′**) Skeletons of P0 littermates, (**B**,**B′**) the atlas, (**C**,**C′**) the axis, (**D**,**D′**) the first thoracic vertebra, (**E**,**E′**) the first lumbar vertebra and (**F**,**F′**) the first sacral vertebra at P0. (A-F,A′-F′) In the mutant, the vertebral arch was partially or completely lost (arrows in B′-F′). (**G**,**G′**) Ventral views of the thoracic to lumber regions. In the mutant, the 13th ribs were only vestigial (arrows in G′). T13, 13th thoracic vertebrae. (**H**,**H′**,**I**,**I′**) Defects of the vertebral arches were also observed in the *Cv2*$^{-/-}$ mutants at E14.5 (H′,I′). Black arrows (H) show the normal vertebral arches. Gray arrows (H′) indicated the vestigial lateral components of the vertebral arches. (**J**,**J′**) In the mutant, the laryngeal cartilages were small (or partially lost) and the bronchial cartilages were completely lost (arrow in A′ and bracket in J′) at P0. (**K**,**K′**) Dorsal views of the skull. In the mutant, the unossified region of the metopic suture was widely opened (arrow in K′). f, frontal bone; p, parietal bone. (**L**,**L′**) Ventral views of the skull base. In the mutant, the basisphenoid (bs) had a cavity in the middle (arrow in L′). bo, basioccipital bone. (**M**,**M′**) Side views of the skull. In the mutant, the retrotympanic process (rp, white arrow in M) of the squamosal bone was lost. st, squamosal temporaris. (**N**,**N′**) In the mutant, the scapula was small or had a hole (arrowhead in N′), and the deltoid tuberosity was lost (arrow in N′). (**O**,**O′**) In the mutant, reduction of the pubic bone body and diastasis of the symphysis were observed (O′). (A-G,A′-G′,J-O,J′-O′) P0, (H,I,H′,I′) E14.5.

Histological analysis showed that the cell-dense region corresponding to the dorsal vertebral arch was replaced with mesenchymal tissues in the null mutant at E14.5 (Fig. 4A-D). By contrast, no obvious histological difference in this region was found between the control and mutant mice at E12.5 (data not shown). Consistent with this finding, the expressions of *Zic1* (an marker for dorsal sclerotome-derived mesenchyme) (Aruga et al., 1999) in the future vertebral arch region was unaffected in the null mutant at E12.5 (Fig. 4I,J). These findings suggest that the loss of *Cv2* prevents the further differentiation of the sclerotome-derived precursor cells between E12.5 and E14.5 in this region.

At E14.5, the sizes of the vertebral bodies (which express *Cv2*; Fig. 2E), but not those of the intervertebral discs (not expressing *Cv2*), were reduced in the *Cv2*$^{-/-}$ mutant (Fig. 3I′, Fig. 4E-H). The early vertebral body marker *Pax1* was expressed normally in E12.5 *Cv2*$^{-/-}$ mice (Fig. 4K,L), suggesting that the defect is unlikely to be attributed to impaired initiation of the sclerotomal tissue formation in the vertebral body. RT-PCR analyses of trunk tissues also showed that there was no obvious change in the expression of the early sclerotomal markers *Pax1* and *Sox9* between the control and the null mutant (Fig. 4M). At E14.5, interestingly, an obvious reduction was seen in the amount of cartilage matrix present in the extracellular space (see reduced intercellular spaces; compare Fig. 4E,F). This phenotype could be interpreted as a defect in cartilage cell maturation, as the mutant vertebral body contained a higher percentage of Ki67-positive immature mitotic cells than the normal one (Fig. 4P-R; 38.8% in the mutant and 18.6% in the wild type, E12.5). No significant increase in apopotosis was observed by the TUNEL assay in the *Cv2*$^{-/-}$ mutants at E14.5 (data not shown).

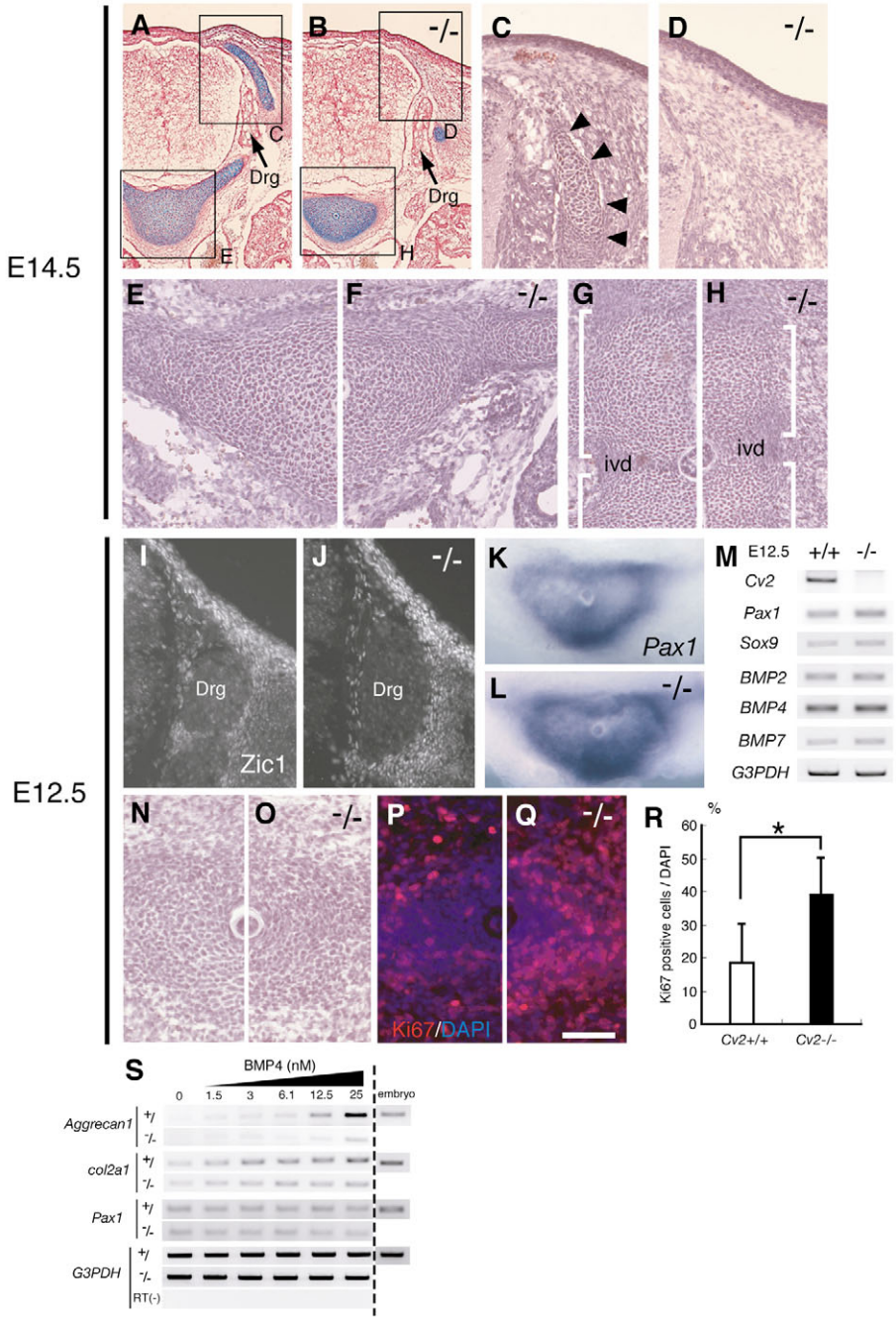

Fig. 4. Requirement of Cv2 for cartilage differentiation in vivo and in vitro. (A-H) E14.5 and (I-R) E12.5. (**A**,**B**) Nuclear Fast Red and Alcian Blue staining of the cross-sections of the trunk region at E14.5. The vertebral arch was lost in the mutant (B). (**C**,**D**) Hematoxylin and Eosin staining of the neighboring sections of A and B (higher magnification views of the vertebral arch region indicated by squares in A and B). The condensed cell mass corresponding to the dorsal vertebral arch cartilage (arrowheads) was replaced with the mesenchymal cells in the mutant (D). (**E**,**F**) The vertebral body was reduced and had less cartilage matrix in the mutant (F). (**G**,**H**) Sagittal sections showed that the rostrocaudal length of the vertebral body was also reduced in the mutant (bracket, compare H with G). ivd, intervertebral disc. (**I**,**J**) Immunostaining of the early dorsal sclerotomal marker Zic1 in the presumptive vertebral arch region showed no reduction in the mutant (J) at E12.5. (**K**,**L**) In situ hybridization analysis of the early sclerotomal gene *Pax1* in the presumptive vertebral body region showed no reduction in the mutant (L). (**M**) RT-PCR analysis of the trunk tissues also showed that the sclerotomal markers *Pax1* and *Sox9* were expressed normally in the mutant at E12.5. The expression levels of the Bmp genes were also unchanged in the mutant. (**N**,**O**) Hematoxylin and Eosin staining of the presumptive vertebral body (surrounding the notochord) in the control (N) and mutant (O) mice. (**P**,**Q**) Ki67 immunostaining. Ki67^{+} mitotic cells were increased in the vertebral body region in the mutant (Q). Scale bar: 50 μm. (**R**) Statistical analysis of P and Q. The percentages of Ki67^{+} cells in the 150 μm × 150 μm square regions surrounding the notochord were presented. The averages ±s.d. (error bars) from three sets of littermates are shown. *P<0.05. (**S**) RT-PCR analysis showed that *Cv2*$^{-/-}$ MEF cells had attenuated responses to Bmp4 for the induction of aggrecan 1 and *Col2a1*.

We next sought to elucidate the mechanism of the Cv2 action as a regulatory signal of skeletal development, focusing on its relation to Bmp signaling. RT-PCR analyses using embryonic trunk tissues (axial and body wall tissues, excluding the internal organs) showed reduced levels of the early cartilage precursor markers aggrecan 1 (Glumoff et al., 1994) and collagen2 α1 (*Col2a1*) (Cheah et al., 1991) in *Cv2*$^{-/-}$ embryos at E14.5 (see Fig. S3 in the supplementary material). By contrast, no significant differences in the transcription levels of Bmp genes (*Bmp2*, *Bmp4* and *Bmp7*) were observed between the control and *Cv2*$^{-/-}$ embryos at E12.5 and E14.5 (Fig. 4M; see Fig. S3 in the supplementary material), suggesting that the *Cv2*$^{-/-}$ phenotypes could not be explained simply by a reduction in the general expression levels of Bmp genes.

As *Cv2*$^{-/-}$ mice showed a significant decrease in the postmitotic mature cartilage cells (Fig. 4P-R), we next studied the functional relationship between Bmp signals and Cv2 in primary culture experiments using MEF cells. We prepared MEF cells from the control and mutant mice, and examined the effects of exogenous Bmp4 on early cartilage markers. Although the expression of aggrecan 1 was induced in a dose-dependent manner by Bmp4 (after 48 hours treatment), *Cv2*$^{-/-}$ MEF cells showed a reduced aggrecan 1 induction when compared with control MEF cells (Fig. 4S, rows 1,2). A similar reduction (albeit moderate) was observed for another early cartilage marker *Col2a1* (Fig. 4S, rows 3,4). In contrast to the induction by Bmp4 proteins, aggrecan 1 induction by a transfected plasmid bearing constitutively-active

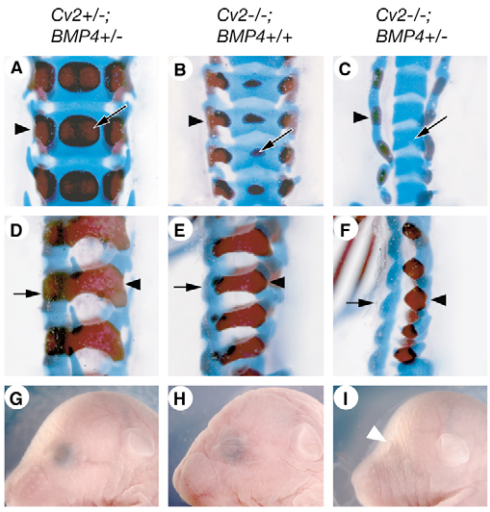

Fig. 5. Genetic enhancement of *Cv2*$^{-/-}$ phenotypes observed by deleting one copy of *Bmp4*. (**A-F**) Skeletal samples of P0 neonates. Lumbar vertebrae. (A-C) Frontal view. (D-F) Left lateral view. Arrow, ossification of the vertebral body; arrowhead, ossifying part of the vertebral arch. (**G-I**) External appearance of P0 neonate heads. Arrowhead, missing eye. *Cv2*$^{+/-}$;*Bmp4*$^{+/-}$ (A,D,G), *Cv2*$^{-/-}$;*Bmp4*$^{+/+}$ (B,E,H) and *Cv2*$^{-/-}$;*Bmp4*$^{+/-}$ (C,F,I) mice.

ALK2 (*CA-ALK2*) was observed at similar levels in control and *Cv2*$^{-/-}$ MEF cells (data not shown), suggesting that Cv2 function is needed for Bmp4-induced aggrecan 1 expression upstream of (or at) the Bmp-receptor level.

Cooperative roles of *Cv2* and *Bmp4* in the development of the vertebrae and eyes

During skeletal development, Bmp ligands are expressed and play essential roles at multiple phases in cartilage and bone differentiation (reviewed by Canalis et al., 2003; Wan and Cao, 2005). For example, the retrovirus-mediated misexpression of noggin in the axial skeleton inhibits the cartilage formation in chick, whereas the expression of *Pax1* is not affected (Murtaugh et al., 1999). Moreover, the *Bmp7*-null mutant, like the *Cv2*$^{-/-}$ mutant, shows the defects of the vertebral arches (Jena et al., 1997). In this respect, the *Cv2*$^{-/-}$ phenotype of cartilage and bone defects (Figs 3, 4) seems consistent with the idea that Cv2 acts in the same direction as Bmp signals.

To obtain direct genetic evidence for either a pro- or anti-Bmp role, we next examined the effect of Bmp attenuation on the *Cv2*$^{-/-}$ mutant phenotype. In particular, we tested whether the vertebral defect, which is a most evident skeletal phenotype, was enhanced or rescued by reducing *Bmp4* gene dose (Fig. 5). Unlike *Cv2*$^{-/-}$ mutants, *Cv2*$^{+/-}$;*Bmp4*$^{+/-}$ mice were externally healthy and fertile, and, consistently, did not show a vertebral phenotype [Fig. 5A,D; no dorsal vertebral defects were observed, unlike those reported for *Bmp4*$^{lacZ/+}$ recently in a different genetic background (Goldman et al., 2006)]. By contrast, the deletion of one copy of *Bmp4* strongly and cooperatively enhanced the vertebral defect of *Cv2*$^{-/-}$ mutants (compare Fig. 5C,F with 5B,E), causing (1) reduction of the vertebral body in size and of its ossification (arrow) and (2) suppression of vertebral arch development (arrowhead). These findings demonstrate that *Bmp4* has strong genetic enhancement with *Cv2*, indicating that *Cv2* and *Bmp4* function cooperatively, rather than antagonistically.

In the external phenotype, the reduction of the *Bmp4* gene dose synergistically increased the frequency of the microphthalamic phenotype. A strong defect was found in 100% of *Cv2*$^{-/-}$; *Bmp4*$^{+/-}$ eyes (n=6), while micropthalmia was seen only in 18% (n=22) and 1.7% (n=172) of *Cv2*$^{+/-}$; *Bmp4*$^{+/-}$ and *Cv2*$^{-/-}$; *Bmp4*$^{+/+}$ eyes, respectively, suggesting that *Cv2* and *Bmp4* work together in the same direction with respect to eye development.

Taken together, these findings show that *Cv2* plays a pro-Bmp role at least in vertebral and eye organogenesis.

Essential role of *Cv2* in kidney development

To further elucidate the role of *Cv2* in Bmp-related organogenesis, we next examined the phenotype of *Cv2*$^{-/-}$ in kidney development, where Bmp signals also play essential roles (Godin et al., 1999; Simic and Vukicevic, 2005). During nephrogenesis, *Bmp4* is expressed in the stromal mesenchyme, S-shaped bodies and paraureteric mesenchyme, whereas *Bmp7* is expressed in the nephrogenic mesenchyme and ureteric bud/collecting duct (Godin et al., 1998; Miyazaki et al., 2000). Small kidneys and decreased numbers of nephrons have been reported for the *Bmp4*$^{+/-}$ and *Bmp7*$^{-/-}$ mutants (Dudley et al., 1995; Luo et al., 1995; Miyazaki et al., 2000). In *Cv2*$^{-/-}$ mice, the size of the kidney was significantly reduced at birth (Fig. 6B). In the section cut along the longest axis, the kidney of the null mutant was 27.0±12.4% smaller (n=6; Fig. 6D) than that of the wild-type mouse (n=6; Fig. 6C). The number of glomeruli was also reduced in the null mutant (by 56.8±9.4%, n=6; also see Fig. 7A, lanes 1, 2), whereas no obvious morphological defect was found in the renal corpuscle (Fig. 6F).

A similar hypomorphic phenotype was also observed for the *Cv2*$^{-/-}$ kidney at E14.5 (Fig. 6G,H) and E18.5 (not shown). During nephrogenesis, strong *Cv2* expression was found in the condensed nephrogenic mesenchyme (Fig. 2H-K) and in the comma- and S-shaped bodies (derivatives of the nephrogenic mesenchyme; Fig. 2H,K). The nephrogenic mesenchyme is known to have a major contribution to the generation of the nephron. At E14.5, the number of *Pax2*-positive masses of condensed nephrogenic mesenchymes was significantly reduced in the *Cv2*$^{-/-}$ kidney (Fig. 6I-K). Immunohistochemical analysis revealed that the general histological arrangement of the Wt1^{+} nephrogenic mesenchyme (and S-shaped bodies) and E-cadherin^{+} collecting ducts was largely unaffected (Fig. 6L,M), although both the number of nephrons and the size of the kidney were reduced.

Taken together, these observations suggest that Cv2 has an essential function for the generation of the proper number of nephrons, presumably by acting on the nephrogenic mesenchymes, which themselves strongly expresses *Cv2*. As the relative reduction in nephron numbers is more evident at P0 than at E14.5 (Fig. 6K, Fig. 7A), the continuous expression of *Cv2* (Fig. 2H-K) may be also necessary during a substantial period of kidney organogenesis after E14.5.

Enhancement of the kidney defect by combining *Cv2*$^{-/-}$ and *Kcp*$^{-/-}$

The kidney defect phenotype of the *Cv2* mutant appears consistent with the idea that *Cv2* plays a positive regulatory role in Bmp signaling. However, previous gene targeting studies have demonstrated that the blockade of Bmp signals (e.g., the lack of *Bmp7*) can cause an even more drastic reduction in kidney development (Dudley et al., 1995; Luo et al., 1995). To test the possibility that some other related molecules act in a partially redundant manner, we next examined the compound phenotypes of *Cv2* and *Kcp* mutants. Like Cv2, Kcp is a Kielin-related

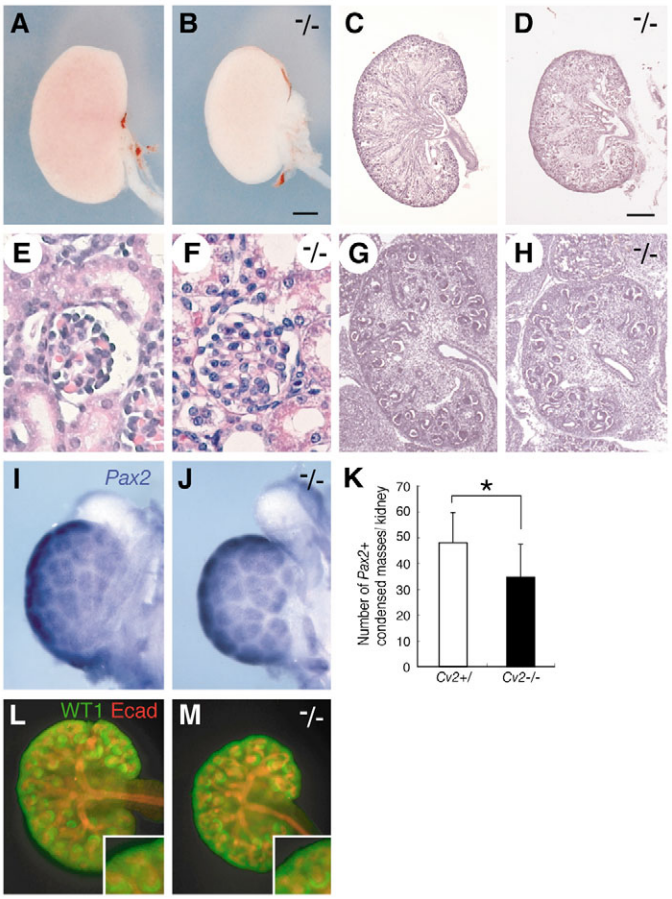

Fig. 6. Kidney defects in the *Cv2* mutant. (**A-D**) External appearances (A,B) and longitudinal sections (C,D; along the longest axis) of the kidneys at P0. Scale bars: 500 μm. Reduced kidney size was observed in the $Cv2^{-/-}$ mutant (B,D). (**E**,**F**) HE staining showed no obvious morphological defects of the renal corpuscle in the $Cv2^{-/-}$ mutant kidney at P0 (F). (**G**,**H**) The kidney was smaller in the $Cv2^{-/-}$ mutant (H) at E14.5. (**I**,**J**) Whole-mount in situ hybridization of *Pax2* expression in the control (I) and mutant (J) kidneys. The *Pax2*-positive condensed mesenchymes were formed in the mutant, but the number was reduced (**K**; $*P<0.05$, *t*-test). (**L**,**M**) WT1-positive condensed mesenchymes and glomerular podocytes (green) and E-cadherin-positive collecting ducts (red) are shown in whole-mount immunostaining. The general architecture of the kidney was largely unaffected in the $Cv2^{-/-}$ mutant (M).

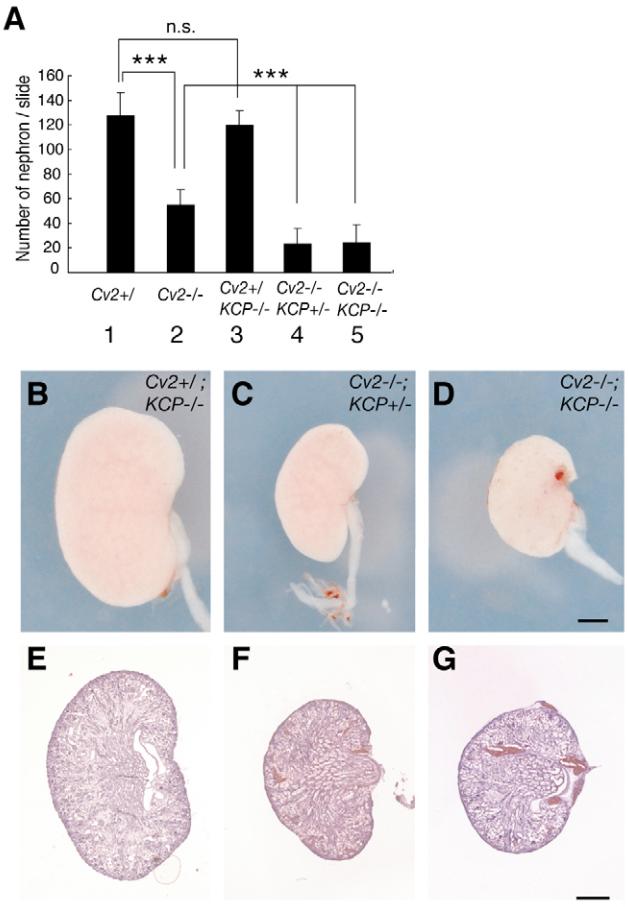

Fig. 7. Kidney defects are enhanced in the *Cv2;Kcp* compound mutant. (**A**) Numbers of the glomeruli in the maximal longitudinal section of the kidney. There was a significant difference between the control and $Cv2^{-/-}$ mutant kidneys. In addition, a significant difference was found between the $Cv2^{-/-}$ mutant with both *Kcp* alleles and that without one or two *Kcp* alleles ($***P<0.001$; Tukey test). Error bars show s.d.; n.s., no significant difference. (**B-G**) External appearances (B-D) and longitudinal sections (E-G; along the longest axis) of the kidneys at P0. Scale bars: 500 μm. (B,E) There was no decrease in size in the $Kcp^{-/-}$ kidney, even on the $Cv2^{+/-}$ background (not shown). (C,D,F,G) The small-kidney phenotype of the $Cv2^{-/-}$ mutant was enhanced on the $Kcp^{+/-}$ and $Kcp^{-/-}$ backgrounds.

molecule that contains multiple Chd-type cysteine-rich repeats, a vWD domain and a TIL domain (see Fig. S1 in the supplementary material), and physically binds to Bmp proteins (Lin et al., 2005). During embryogenesis, *Kcp* is expressed in the nephric duct and the mesonephric tubule (E9-10) and in the presumptive metanephric tubules (E16) (data not shown) (Lin et al., 2005). Luciferase assays in 3T3 cells have suggested a pro-Bmp activity for Kcp (Lin et al., 2005).

We generated $Kcp^{-/-}$ mice by gene disruption, and found that the $Kcp^{-/-}$ mice were viable and fertile. They exhibited no gross structural defects, including in kidney formation (Fig. 7B and data not shown), consistent with a recent report (Lin et al., 2005).

Interestingly, a substantial enhancement in the kidney defect was seen when the *Cv2* and *Kcp* mutants were crossed. On the $Cv2^{+/+}$ or $Cv2^{+/-}$ background, the loss of both *Kcp* alleles exhibited no obvious effects on kidney formation (Fig. 7A, lane 3 and Fig. 7B). On the $Cv2^{-/-}$ background, however, the additional deletion of one or both alleles of *Kcp* caused a further reduction in kidney size (Fig. 7C,D,F,G) and the glomerulus number (Fig. 7A, lanes 4, 5). Furthermore, the kidney of the $Cv2^{-/-}$;$Kcp^{+/-}$ or $Cv2^{-/-}$;$Kcp^{-/-}$ mutant exhibited strong disorganization of the cortex-medullar arrangement with no clear border in between (Fig. 7F,G; a minor disorganization was also seen in the $Cv2^{-/-}$ mutant alone; Fig. 6D). These findings of genetic interactions indicate that both *Cv2* and *Kcp* function in the same direction to promote kidney development, and that these Cv2-related proteins play a major regulatory role for the morphogenetic signals of kidney development.

By contrast, the skeletal phenotypes of the $Cv2^{-/-}$ mutant were not enhanced by the additional deletion of both *Kcp* alleles (data not shown). It is consistent with the fact that strong *Kcp* expression is not detected in the skeletal tissues (M.I. and Y.S., unpublished).

DISCUSSION

This study has demonstrated that *Cv2* is essential for multiple organogenetic processes that involve Bmp signals. The null mutant phenotypes of *Cv2* are in accordance with the idea of pro-Bmp functions of Cv2 in mammalian organogenesis such as vertebral and eye development.

Mutant phenotypes indicate essential roles of *Cv2* as a pro-Bmp factor in skeletal and eye organogenesis

A number of previous reports have shown that Bmp signals play positive regulatory roles in cartilage and bone differentiation. The $Cv2^{-/-}$ mice exhibit major trunk defects and minor head deformities in their cartilages and bones (Fig. 3; see Table S2 in the supplementary material), which express *Cv2* (Fig. 2 and data not shown). In the trunk, severe defects are seen in both the axial structures (e.g. the vertebral body and arch) and the non-axial structures (e.g. the 13th rib, pharyngeal and tracheal cartilages, scapula, deltoid tuberosity of the humerus and unclosed symphysis) (Fig. 3G′,J′,N′,O′; see Table S2 in the supplementary material). In addition, minor malformations are found in the head, including the presence of a cavity in the basisphenoid bone, small interparietal and supraoccipital bones, and an enlargement of the metopic suture (Fig. 3K′,L′; see Table S2 in the supplementary material).

Importantly, many aspects of these $Cv2^{-/-}$ phenotypes (including minor defects) coincide with those found in other mutant mice with attenuated Bmp signaling. For example, like the $Cv2^{-/-}$ mouse, the *Bmp7* mutant has a small basisphenoid with a cavity (Luo et al., 1995; Jena et al., 1997) and a partial loss of the vertebral arches (Jena et al., 1997). The *Bmpr2* mutant mouse (hypomorphic allele) lacks the 13th ribs and has malformed interparietal bones (Delot et al., 2003), as is seen with the $Cv2^{-/-}$ mouse. The deltoid tuberosity is also lost in $Bmp7^{-/-}$;$Bmpr1b^{-/-}$ mutants (Yi et al., 2000). The enlarged metopic suture is found in $Bmp1^{-/-}$ mice (Suzuki et al., 1996).

These phenotypes are thus consistent with a pro-Bmp role of Cv2 in skeletal development. Moreover, our findings of genetic enhancement of *Cv2* and *Bmp4* mutants strongly support this idea. To further exclude the possibility of having any anti-Bmp function (particularly as a minor contribution), it may be useful in future studies to examine the *Cv2* mutant phenotypes in detail on backgrounds mutant for other Bmp pathway genes. In this respect, one complex problem is how to explain the vertebral defect in the null *Chd* mutant (Bachiller et al., 2003), which is similar to the defective formation found in $Cv2^{-/-}$ and $Bmp7^{-/-}$ mutants. In addition, the null mutant of *Tsg*, which encodes a Chd co-factor, also exhibits a similar vertebral defect (Nosaka et al., 2003; Petryk et al., 2004; Zakin and De Robertis, 2004). As Tsg has been shown to act as a pro-Bmp factor at least in some developmental contexts (Zakin and De Robertis, 2004; Zakin et al., 2005), a possible pro-Bmp role of *Chd* in mouse vertebral development may be an intriguing topic that should be tested genetically in the future.

Essential roles of Cv2 in other aspects of Bmp-related organogenesis

Parallels between the *Cv2* mutant and the Bmp-related mutants are also found in the kidney phenotypes. Renal hypoplasia with decreased nephrons is observed in $Bmp4^{+/-}$ and $Bmp7^{-/-}$ mice, respectively (Dudley et al., 1995; Luo et al., 1995; Miyazaki et al., 2000), as is seen in the *Cv2* mutant (Figs 6, 7). The hypoplastic phenotype of the kidney in the *Cv2* mutant is further enhanced by combining it with a mutation of *Kcp* (Fig. 7A), which encodes a secreted protein belonging to the Cv2/kielin subfamily. As a recent report has indicated that Kcp acts as a pro-Bmp factor at least in vitro (Lin et al., 2005), these findings further support the idea that Cv2 acts as a positive regulator of Bmp signals. However, the conclusion on the pro-Bmp role of Cv2 in nephrogenesis should await further genetic crossing studies with mutants of Bmp-related genes in the future, as we have so far failed to observe a more drastic renal phenotype in $Cv2^{-/-}$;$Bmp4^{+/-}$ mice beyond the simple additive effect (our preliminary observations).

Are there differential roles for Cv2 and Kcp in renal development? In fact, the kidney develops normally in the *Kcp*-null mutant, even in the $Cv2^{+/-}$ background (Fig. 7B,E; M.I. and Y.S., unpublished) (Lin et al., 2005). Interestingly, the recent report showed that $Kcp^{-/-}$ mice are more susceptible to developing renal fibrosis and pathological tubular lesions after injury (Lin et al., 2005). This raises the interesting possibility that Cv2 plays a predominant role in the organogenesis of the embryonic kidney while Kcp is an essential regulator of renal tissue maintenance/regeneration after birth. Detailed analyses will be required in future studies to elucidate the exact relationship between these two Cv2/kielin-related factors.

In addition to renal hypoplasia, the *Cv2*-null mutant has the impaired maturation and expansion of the alveoli (see Fig. S4 in the supplementary material; rather than differentiation of each cellular components), which are reminiscent of a phenotype in the transgenic mice with a dominant-negative *Bmpr1b* overexpressed in the lung (Weaver et al., 1999; Weaver et al., 2003). Therefore, a possible pro-Bmp role of Cv2 in lung development should be also an intriguing topic for future investigation.

The function of Cv2 is not essential for all Bmp-dependent embryonic processes

This null mutant study has also indicated that Cv2 is not required for several other aspects of Bmp-dependent developmental processes. For example, the lack of Cv2 causes strong defects of cartilage and bone development, but not in all skeletal parts. Even in vertebral development, which is clearly defective, *Cv2* is not needed for the early Bmp-dependent events of cartilage formation, such as the induction of early precursor markers (e.g. *Pax1*, *Zic1*, *Sox9*).

Moreover, *Cv2* seems dispensable for developmental events during the early gestation period such as gastrulation and early neural patterning. At E12.5, the $Cv2^{-/-}$ mice exhibit no remarkable gross defects and are found in a Mendelian ratio (see Table S1 in the supplementary material; M.I. and Y.S., unpublished), even though *Cv2* is expressed in the rostral mesoderm and the caudal primitive streak during gastrulation (Coffinier et al., 2002).

The dorsoventral patterning of the neural tube is another example that is dependent on Bmp signals [emanating from the roof plate and overlying ectoderm (Lee and Jessell, 1999)] and is not affected in $Cv2^{-/-}$ mutants. The dorsoventral markers of the neural tube (e.g. Msx1/2, Pax7, Isl1, Mash1 and Hnf3b) are normally expressed in $Cv2^{-/-}$ mice at E10.5 (see Fig. S5 in the supplementary material). In addition, the interdigital shaping of the hand appears normal in $Cv2^{-/-}$ mice (Fig. 1E and data not shown), although this region expresses both *Cv2* and *Bmp2/4* (Kamimura et al., 2004). These findings indicate that the requirement for *Cv2* is stage- and tissue-dependent in mouse embryogenesis.

Bmp signaling enhancement by Cv2 proteins

The mechanism by which Cv2 enhances Bmp signals remains to be clarified in the future. Several possibilities can be considered for the mode of the Cv2 action at the molecular level. These include (1)

enhancement of the binding between Bmp proteins and their receptors by Cv2 proteins, (2) competition with Bmp-binding inhibitors such as chordin and noggin for Bmp proteins, (3) control of the matrix-association/sequestration of Bmp, and (4) protection of the Bmp proteins from degradation (proteases).

In favor of the first model, a recent study suggested that the Cv2/kielin –related protein Kcp enhances the binding of the Bmp protein and its receptor by forming a tertiary complex (Lin et al., 2005). However, an extensive biochemical study using Biacore analysis did not seem to support the mechanism of the enhanced receptor binding of Bmps by Cv2 proteins (Rentzsch et al., 2006). Instead, the study demonstrated that Cv2 and Chd proteins compete each other for Bmp proteins as their binding partners. In fact, as epistatic analysis in zebrafish dorsoventral patterning has indicated that the Cv2 morphant phenotypes consist of both Chd-dependent and Chd-independent components, the Bmp signaling enhancement by Cv2 may involve more than one mechanism.

Previous in vitro studies have demonstrated that vertebrate Cv2 proteins bind to Bmp2, Bmp4, Bmp6 and Bmp7 with a high affinity, but not to Gdf5 (Moser et al., 2003; Coles et al., 2004; Rentzsch et al., 2006). Although the present study implies strong functional interactions between Cv2 and Bmp4, the Cv2-binding specificity among the Bmp/Tgfβ superfamily ligands should be an important topic to be analyzed in the in vivo context.

We are grateful to M. Hibi, H. Enomoto and H. Inomata for invaluable comments, to K. Miyazono, H. Beppu, T. Kitamura, and T. Nosaka for discussion on Bmp-related mutants, to F. Osakada for help in the statistical analysis, and to K. Furushima and T. Uesaka for technical advice. MI is thankful to Ayumi Ikeya for constant encouragement and support during this study. This work was supported by grants-in-aid (YS) from the Ministry of Education, Culture, Sports, Science and Technology, the Kobe Cluster Project and the Leading Project.

Supplementary material

Supplementary material for this article is available at http://dev.biologists.org/cgi/content/full/133/22/4463/DC1

References

Aruga, J., Mizugishi, K., Koseki, H., Imai, K., Balling, R., Noda, T. and Mikoshiba, K. (1999). Zic1 regulates the patterning of vertebral arches in cooperation with Gli3. *Mech. Dev.* **89**, 141-150.

Ashe, H. L. and Levine, M. (1999). Local inhibition and long-range enhancement of Dpp signal transduction by Sog. *Nature* **398**, 427-431.

Bachiller, D., Klingensmith, J., Shneyder, N., Tran, U., Anderson, R., Rossant, J. and De Robertis, E. M. (2003). The role of chordin/Bmp signals in mammalian pharyngeal development and DiGeorge syndrome. *Development* **130**, 3567-3578.

Binnerts, M. E., Wen, X., Cante-Barrett, K., Bright, J., Chen, H. T., Asundi, V., Sattari, P., Tang, T., Boyle, B., Funk, W. et al. (2004). Human Crossveinless-2 is a novel inhibitor of bone morphogenetic proteins. *Biochem. Biophys. Res. Commun.* **315**, 272-280.

Canalis, E., Economides, A. N. and Gazzerro, E. (2003). Bone morphogenetic proteins, their antagonists, and the skeleton. *Endocr. Rev.* **24**, 218-235.

Cheah, K. S., Lau, E. T., Au, P. K. and Tam, P. P. (1991). Expression of the mouse alpha 1(II) collagen gene is not restricted to cartilage during development. *Development* **111**, 945-953.

Coffinier, C., Ketpura, N., Tran, U., Geissert, D. and De Robertis, E. M. (2002). Mouse Crossveinless-2 is the vertebrate homolog of a Drosophila extracellular regulator of BMP signaling. *Mech. Dev.* **119**, S179-S184.

Coles, E., Christiansen, J., Economou, A., Bronner-Fraser, M. and Wilkinson, D. G. (2004). A vertebrate crossveinless 2 homologue modulates BMP activity and neural crest cell migration. *Development* **131**, 5309-5317.

Conley, C. A., Silburn, R., Singer, M. A., Ralston, A., Rohwer-Nutter, D., Olson, D. J., Gelbart, W. and Blair, S. S. (2000). Crossveinless 2 contains cysteine-rich domains and is required for high levels of BMP-like activity during the formation of the cross veins in Drosophila. *Development* **127**, 3947-3959.

Dale, L., Howes, G., Price, B. M. J. and Smith, J. C. (1992). Bone morphogenetic protein 4, a ventralizing factor in early Xenopus development. *Development* **115**, 573-585.

Decotto, E. and Ferguson, E. L. (2001). A positive role for Short gastrulation in modulating BMP signaling during dorsoventral patterning in the Drosophila embryo. *Development* **128**, 3831-3841.

Delot, E. C., Bahamonde, M. E., Zhao, M. and Lyons, K. M. (2003). BMP signaling is required for septation of the outflow tract of the mammalian heart. *Development* **130**, 209-220.

De Robertis, E. M. and Sasai, Y. (1996). A common plan for dorsoventral patterning in Bilateria. *Nature* **380**, 37-40.

Dudley, A. T., Lyons, K. M. and Robertson, E. J. (1995). A requirement for bone morphogenetic protein-7 during development of the mammalian kidney and eye. *Genes Dev.* **9**, 2795-2807.

Fainsod, A., Steinbeisser, H. and De Robertis, E. M. (1994). On the function of BMP-4 in patterning the marginal zone of the Xenopus embryo. *EMBO J.* **13**, 5015-5025.

Ferguson, E. L. and Anderson, K. (1992a). decapentaplegic acts as a morphogen to organize dorsal-ventral pattern in the Drosophila embryo. *Cell* **71**, 451-461.

Ferguson, E. L. and Anderson, K. (1992b). Localized enhancement and repression of the activity of the TGF-beta family member, decapentaplegic, is necessary for dorso-ventral pattern formation in the Drosophila embryo. *Development* **114**, 583-597.

Fisher, S., Amacher, S. L. and Halpern, M. E. (1997). Loss of cerebrum function ventralizes the zebrafish embryo. *Development* **124**, 1301-1311.

François, V., Solloway, M., O'Neill, J. W., Emery, J. and Bier, E. (1994). Dorsal-ventral patterning of the Drosophila embryo depends on a putative negative growth factor encoded by the shortgastrulation gene. *Genes Dev.* **8**, 2602-2616.

Garcia-Bellido, A. and de Celis, J. F. (1992). Developmental genetics of the venation pattern of Drosophila. *Annu. Rev. Genet.* **26**, 277-304.

Glinka, A., Wu, W., Onichtchouk, D., Blumenstock, C. and Niehrs, C. (1997). Head induction by simultaneous repression of Bmp and Wnt signalling in Xenopus. *Nature* **389**, 517-519.

Glumoff, V., Savontaus, M., Vehanen, J. and Vuorio, E. (1994). Analysis of aggrecan and tenascin gene expression in mouse skeletal tissues by northern and in situ hybridization using species specific cDNA probes. *Biochim. Biophys. Acta* **1219**, 613-622.

Godin, R. E., Takaesu, N. T., Robertson, E. J. and Dudley, A. T. (1998). Regulation of BMP7 expression during kidney development. *Development* **125**, 3473-3482.

Godin, R. E., Robertson, E. J. and Dudley, A. T. (1999). Role of BMP family members during kidney development. *Int. J. Dev. Biol.* **43**, 405-411.

Goldman, D. C., Hackenmiller, R., Nakayama, T., Sopory, S., Wong, C., Kulessa, H. and Christian, J. L. (2006). Mutation of an upstream cleavage site in the BMP4 prodomain leads to tissue-specific loss of activity. *Development* **133**, 1933-1942.

Grieshammer, U., Cebrian, C., Ilagan, R., Meyers, E., Herzlinger, D. and Martin, G. R. (2005). FGF8 is required for cell survival at distinct stages of nephrogenesis and for regulation of gene expression in nascent nephrons. *Development* **132**, 3847-3857.

Gurdon, J. B. and Bourillot, P. Y. (2001). Morphogen gradient interpretation. *Nature* **413**, 797-803.

Hammerschmidt, M. and Mullins, M. C. (2002). Dorsoventral patterning in the zebrafish: bone morphogenetic proteins and beyond. In *Pattern Formation in Zebrafish* (ed. L. Solnica-Krezel), pp. 72-95. Berlin, Heidelberg: Springer-Verlag

Hemmati-Brivanlou, A., Kelly, O. G. and Melton, D. A. (1994). Follistatin, an antagonist of activin is expressed in the Spemann organizer and displays direct neuralizing activity. *Cell* **77**, 283-295.

Hogan, B. L. (1996). Bone morphogenetic proteins: multifunctional regulators of vertebrate development. *Genes Dev.* **10**, 1580-1594.

Hogan, B., Beddington, R., Costantini, F. and Lacy, E. (1994). *Manipulating the Mouse Embryo* (2nd edn). Cold Spring Harbor, NY: Cold Spring Harbor Laboratory Press.

Hsu, D. R., Economides, A. N., Wang, X., Eimon, P. M. and Harland, R. M. (1998). The Xenopus dorsalizing factor Gremlin identifies a novel family of secreted proteins that antagonize BMP activities. *Mol. Cell* **1**, 673-683.

Ikeya, M. and Takada, S. (1998). Wnt signaling from the dorsal neural tube is required for the formation of the medial dermomyotome. *Development* **125**, 4969-4976.

Ikeya, M., Kawada, M., Nakazawa, Y., Sakuragi, M., Sasai, N., Ueno, M., Kiyonari, H., Nakao, K. and Sasai, Y. (2005). Gene disruption/knock-in analysis of mONT3: vector construction by employing both in vivo and in vitro recombinations. *Int. J. Dev. Biol.* **49**, 807-823.

Jena, N., Martin-Seisdedos, C., McCue, P. and Croce, C. M. (1997). BMP7 null mutation in mice: developmental defects in skeleton, kidney, and eye. *Exp. Cell Res.* **230**, 28-37.

Jones, C. M., Lyons, K. M., Lapan, P. M., Wright, C. V. E. and Hogan, B. L. M. (1992). DVR-4 (bone morphogenetic protein-4) as a posterior-ventralizing factor in Xenopus mesoderm induction. *Development* **115**, 639-647.

Kamimura, M., Matsumoto, K., Koshiba-Takeuchi, K. and Ogura, T. (2004). Vertebrate crossveinless 2 is secreted and acts as an extracellular modulator of the BMP signaling cascade. *Dev. Dyn.* **230**, 434-445.

Lamb, T. M., Knecht, A. K., Smith, W. C., Stachel, S. E., Economides, A. N.,

Stahl, N., Yancopolous, G. D. and Harland, R. M. (1993). Neural induction by the secreted polypeptide noggin. *Science* **262**, 713-718.
Larrain, J., Bachiller, D., Lu, B., Agius, E., Piccolo, S. and De Robertis, E. M. (2000). BMP-binding modules in chordin: a model for signalling regulation in the extracellular space. *Development* **127**, 821-830.
Lawson, K. A., Dunn, N. R., Roelen, B. A., Zeinstra, L. M., Davis, A. M., Wright, C. V., Korving, J. P. and Hogan, B. L. (1999). Bmp4 is required for the generation of primordial germ cells in the mouse embryo. *Genes Dev.* **13**, 424-436.
Lee, K. J. and Jessell, T. M. (1999). The specification of dorsal cell fates in the vertebrate central nervous system. *Annu. Rev. Neurosci.* **22**, 261-294.
Lengner, C. J., Lepper, C., van Wijnen, A. J., Stein, J. L., Stein, G. S. and Lian, J. B. (2004). Primary mouse embryonic fibroblasts: a model of mesenchymal cartilage formation. *J. Cell Physiol.* **200**, 327-333.
Lin, J., Patel, S. R., Cheng, X., Cho, E. A., Levitan, I., Ullenbruch, M., Phan, S. H., Park, J. M. and Dressler, G. R. (2005). Kielin/chordin-like protein, a novel enhancer of BMP signaling, attenuates renal fibrotic disease. *Nat. Med.* **11**, 387-393.
Luo, G., Hofmann, C., Bronckers, A. L., Sohocki, M., Bradley, A. and Karsenty, G. (1995). BMP-7 is an inducer of nephrogenesis, and is also required for eye development and skeletal patterning. *Genes Dev.* **9**, 2808-2820.
Massague, J. and Chen, Y. G. (2000). Controlling TGF-beta signaling. *Genes Dev.* **14**, 627-644.
Matsui, M., Mizuseki, K., Nakatani, J., Nakanishi, S. and Sasai, Y. (2000). Xenopus kielin: A dorsalizing factor containing multiple chordin-type repeats secreted from the embryonic midline. *Proc. Natl. Acad. Sci. USA* **97**, 5291-5296.
Miyazaki, Y., Oshima, K., Fogo, A., Hogan, B. L. and Ichikawa, I. (2000). Bone morphogenetic protein 4 regulates the budding site and elongation of the mouse ureter. *J. Clin. Invest.* **105**, 863-873.
Mizuseki, K., Sakamoto, T., Watanabe, K., Muguruma, K., Ikeya, M., Nishiyama, A., Arakawa, A., Suemori, H., Nakatsuji, N., Kawasaki, H. et al. (2003). Generation of neural crest-derived peripheral neurons and floor plate cells from mouse and primate embryonic stem cells. *Proc. Natl. Acad. Sci. USA* **100**, 5828-5833.
Moser, M., Binder, O., Wu, Y., Aitsebaomo, J., Ren, R., Bode, C., Bautch, V. L., Conlon, F. L. and Patterson, C. (2003). BMPER, a novel endothelial cell precursor-derived protein, antagonizes bone morphogenetic protein signaling and endothelial cell differentiation. *Mol. Cell. Biol.* **23**, 5664-5679.
Murtaugh, L. C., Chyung, J. H. and Lassar, A. B. (1999). Sonic hedgehog promotes somitic chondrogenesis by altering the cellular response to BMP signaling. *Genes Dev.* **13**, 225-237.
Nosaka, T., Morita, S., Kitamura, H., Nakajima, H., Shibata, F., Morikawa, Y., Kataoka, Y., Ebihara, Y., Kawashima, T., Itoh, T. et al. (2003). Mammalian twisted gastrulation is essential for skeleto-lymphogenesis. *Mol. Cell. Biol.* **23**, 2969-2980.
O'Connor, M. B., Umulis, D., Othmer, H. G. and Blair, S. S. (2006). Shaping BMP morphogen gradients in the Drosophila embryo and pupal wing. *Development* **133**, 183-193.
Parr, B. A. and McMahon, A. P. (1995). Dorsalizing signal Wnt-7a required for normal polarity of D-V and A-P axes of mouse limb. *Nature* **374**, 350-353.
Petryk, A., Anderson, R. M., Jarcho, M. P., Leaf, I., Carlson, C. S., Klingensmith, J., Shawlot, W. and O'Connor, M. B. (2004). The mammalian twisted gastrulation gene functions in foregut and craniofacial development. *Dev. Biol.* **267**, 374-386.
Ralston, A. and Blair, S. S. (2005). Long-range Dpp signaling is regulated to restrict BMP signaling to a crossvein competent zone. *Dev. Biol.* **280**, 187-200.
Rentzsch, F., Zhang, J., Kramer, C., Sebald, W. and Hammerschmidt, M. (2006). Crossveinless 2 is an essential positive feedback regulator of Bmp signaling during zebrafish gastrulation. *Development* **133**, 801-811.
Sasai, Y., Lu, B., Steinbeisser, H., Geissert, D., Gont, L. K. and De Robertis, E. M. (1994). Xenopus chordin: a novel dorsalizing factor activated by organizer-specific homeoboxes genes. *Cell* **79**, 779-790.
Sasai, Y., Lu, B., Steinbeisser, H. and De Robertis, E. M. (1995). Regulation of neural induction by the chd and BMP-4 antagonistic patterning signals in Xenopus. *Nature* **376**, 333-336.
Schulte-Merker, S., Lee, K. J., McMahon, A. P. and Hammerschmidt, M. (1997). The zebrafish organizer requires chordino. *Nature* **387**, 862-863.
Simic, P. and Vukicevic, S. (2005). Bone morphogenetic proteins in development and homeostasis of kidney. *Cytokine Growth Factor Rev.* **16**, 299-308.
Smith, W. C. and Harland, R. M. (1992). Expression cloning of noggin, a new dorsalizing factor localized to the Spemann organizer in Xenopus embryos. *Cell* **70**, 829-840.
Su, H. L., Muguruma, K., Matsuo-Takasaki, M., Kengaku, M., Watanabe, K. and Sasai, Y. (2006). Generation of cerebellar neuron precursors from embryonic stem cells. *Dev. Biol.* **290**, 287-296.
Suzuki, N., Labosky, P. A., Furuta, Y., Hargett, L., Dunn, R., Fogo, A. B., Takahara, K., Peters, D. M., Greenspan, D. S. and Hogan, B. L. (1996). Failure of ventral body wall closure in mouse embryos lacking a procollagen C-proteinase encoded by Bmp1, a mammalian gene related to Drosophila tolloid. *Development* **122**, 3587-3595.
Wagner, D. S. and Mullins, M. C. (2002). Modulation of BMP activity in dorsalventral pattern formation by the chordin and ogon antagonists. *Dev. Biol.* **245**, 109-123.
Wan, M. and Cao, X. (2005). BMP signaling in skeletal development. *Biochem. Biophys. Res. Commun.* **328**, 651-657.
Weaver, M., Yingling, J. M., Dunn, N. R., Bellusci, S. and Hogan, B. L. (1999). Bmp signaling regulates proximal-distal differentiation of endoderm in mouse lung development. *Development* **126**, 4005-4015.
Weaver, M., Batts, L. and Hogan, B. L. (2003). Tissue interactions pattern the mesenchyme of the embryonic mouse lung. *Dev. Biol.* **258**, 169-184.
Wharton, K. A., Ray, R. P. and Gelbart, W. M. (1993). The activity gradient of decapentaplegic is necessary for the specification of dorsal pattern elements in the Drosophila embryo. *Development* **117**, 807-822.
Yagi, T., Tokunaga, T., Furuta, Y., Nada, S., Yoshida, M., Tsukada, T., Saga, Y., Takeda, N., Ikawa, Y. and Aizawa, S. (1993a). A novel ES cell line, TT2, with high germline-differentiating potency. *Anal. Biochem.* **214**, 70-76.
Yagi, T., Nada, S., Watanabe, N., Tamemoto, H., Kohmura, N., Ikawa, Y. and Aizawa, S. (1993b). A novel negative selection for homologous recombinants using diphtheria toxin A fragment gene. *Anal. Biochem.* **214**, 77-86.
Yi, S. E., Daluiski, A., Pederson, R., Rosen, V. and Lyons, K. M. (2000). The type I BMP receptor BMPRIB is required for chondrogenesis in the mouse limb. *Development* **127**, 621-630.
Zakin, L. and De Robertis, E. M. (2004). Inactivation of mouse Twisted gastrulation reveals its role in promoting Bmp4 activity during forebrain development. *Development* **131**, 413-424.
Zakin, L., Reversade, B., Kuroda, H., Lyons, K. M. and De Robertis, E. M. (2005). Sirenomelia in Bmp7 and Tsg compound mutant mice: requirement for Bmp signaling in the development of ventral posterior mesoderm. *Development* **132**, 2489-2499.
Zusman, S. B., Sweeton, D. and Wieschaus, E. F. (1988). short-gastrulation, a mutation causing delays in stage-specific cell shape changes during gastrulation in Drosophila melanogaster. *Dev. Biol.* **129**, 417-442.

Table S1. Number of mice with each genotype in *Cv2*$^{+/-}$ intercrossing

	Cv2		
	+/+	+/–	–/–
E12.5	35 (24.6)	77 (54.2)	30 (21.1)
E14.5	28 (22.8)	69 (56.1)	26 (21.1)
E18.5	11 (33.3)	14 (42.4)	8 (24.2)
P0	9 (21.4)	21 (50.0)	12 (28.6)*
Adult	40 (37.0)	68 (63.0)	0 (0)

*All the neonates died soon after birth.
Percentages are given in parentheses.

Table S2. Penetrance of skeletal abnormalities in *Cv2*$^{-/-}$ mice

		Cv2	
	Phenotypes	+/+ or +/– (*n*=15)	–/– (*n*=9)
Metopic suture	Normal	15	0
	Less ossified	0	9
Interparietal bone	Normal	15	0
	Small	0	9
Supraoccipital bone	Normal	15	0
	Small	0	4
	Small, not ossified	0	5
Basisphenoid	Normal	15	0
	Presence of cavity	0	9
Retrotympanic process of the squamosal bone	Normal	15	0
	Lost	0	9
Laryngeal cartilage	Normal	15	0
	Malformed*	0	9
Bronchial cartilage	Normal	15	0
	Lost	0	9
Vertebral arch	Normal	15	0
	Lost†	0	9
Rib	Normal	15	0
	Thinner	0	9
Rib (T13)	Normal	15	0
	No ribs attached	0	9
Scapula	Normal	15	2
	Malformed	0	7
Deltoid tuberosity	Normal	15	0
	Lost	0	9
Symphysis of the pubic bone	Normal	15	6
	Diastasis	0	3

*Laryngeal cartilage malformation: the lessor horn was almost lost, the greater horn was slightly reduced and the thyroid cartilage was hollow in 100% (nine out of nine) of the mutant.

†The arch of the 2nd cervical vertebra was lost in 33% (three in nine), almost lost in 22% (two in nine) and rudimental in 44% (four out of nine).